



An optimized stator and rotor design of squirrel cage induction motor for EMU train

Hilda Luthfiyah^{a,*}, Okghi Adam Qowiy^a, Arga Iman Malakani^b,
Dwi Handoko Arthanto^c, Fauzi Dwi Setiawan^a, Teddy Anugrah Ramanel^d,
Gilang Mantara Putra^e, Syamsul Kamar^a, Asep Andi Suryandi^{f,g}

^a Research Center for Transposition Technology, National Research and Innovation Agency (BRIN)
PUSPIPTEK, South Tangerang City, Indonesia

^b Research Center for Hydronamics Technology, National Research and Innovation Agency (BRIN)
Jl. Hidrodinamika, Surabaya, 60112, Indonesia

^c Research Center for Accelerator Technology, National Research and Innovation Agency (BRIN)
PUSPIPTEK, South Tangerang City, Indonesia

^d Research Center for Energy Conversion and Conservation, National Research and Innovation Agency (BRIN)
PUSPIPTEK, South Tangerang City, Indonesia

^e Research Center for Artificial Intelligence and Cyber Security, National Research and Innovation Agency (BRIN)
PUSPIPTEK, South Tangerang City, Indonesia

^f Research Center for Process and Manufacturing Industry Technology, National Research and Innovation Agency (BRIN)
PUSPIPTEK, South Tangerang City, Indonesia

^g Electrical and Electronic Engineering, The University of Manchester
Office 40, MECD Eng A - 5th Floor, PO Box 88, Manchester M13 9PL, United Kingdom

Received 17 November 2022; 1st revision 21 December 2022; 2nd revision 6 February 2023; Accepted 3 March 2023;
Published online 31 July 2023

Abstract

This paper aims to objectively calculate the 480-kW squirrel cage induction motor (SCIM) design for the electric multiple unit (EMU) trains. This is done by optimizing the stator slot and rotor slot design to get efficiency and power factor targets. The stator slot design is achieved by limiting the width and height of the stator slot pitch according to the specified range. A depth-to-width ratio is used according to the range to optimize the design of the rotor bar slot. The design process of the induction motor consists of three steps: it determines the specification design target, calculates the specified parameters of the induction motor, and simulates the design to obtain the most optimal motor design using ANSYS Maxwell. The simulation performance values obtained an efficiency of 92.547 % and a power factor of 0.915. This value is obtained from the optimization of the rotor slot and has met the minimum requirements of efficiency and power factor in designing a SCIM. The design proposed in this paper can be developed and applied in the Indonesian domestic railway manufacturing industry.

Copyright ©2023 National Research and Innovation Agency. This is an open access article under the CC BY-NC-SA license (<https://creativecommons.org/licenses/by-nc-sa/4.0/>).

Keywords: squirrel cage induction motor; stator slot; rotor slot; motor efficiency; motor power factor.

I. Introduction

Railways with electric-powered trains use a distributed traction system known as electric multiple unit (EMU). EMU has several advantages, such as low energy consumption with the pollution-free operation, good traction and braking performance, and operational reliability with optimal

redundancy [1][2]. An induction motor (IM) is a type of motor that is reliable to be applied in EMU trains. This characteristic has made them the first choice of train designers and builders [3]. Most IM are chosen as electric vehicle engines because they are known for their sturdy construction, cheaper production costs, and ease of control [4]. In particular, the type of motor widely used for the train propulsion system is squirrel cage induction motor (SCIM). The advantage of SCIM is it has a smaller size and lighter weight than other types of motors, e.g. DC motor, wound

* Corresponding Author. Tel: +62-8563159453
E-mail address: hilda.luthfiyah@brin.go.id

rotor induction motor (WRIM), and wound rotor synchronous motor (WRSM). In addition, SCIM has minimal ground disturbance for the traction motor due to the removal of brushes and commutator. The effect of removing the instrument is that it can save costs and reduce maintenance time [5].

Research on the optimization of IM design in electric-powered trains has grown rapidly. Among them is IM design optimization on stator slots, rotor slots, and rotor shafts with finite element analysis (FEM) analysis using MATLAB [6][7][8]. With the same tools MATLAB, IM optimization was done with air gap variations to get the best efficiency and power factor [9]. In other research, design optimization IM was done by selecting slot types and materials to achieve optimal motor efficiency and performance using different tools, namely ANSYS Maxwell [10][11]. Another method was introduced for motor optimization using the Taguchi and Fuzzy optimization method sequentially [12].

In Indonesian railways, an electric-based railway drive system has been implemented. The current EMU trains in Indonesia use traction motors with output power 100 kW and 180 kW [13][14]. Another type of electric train used in Indonesia is diesel electric multiple unit (DEMU) which uses a traction motor with 550 kW output power [15]. High speed train (HST) in the world, which has a speed of 250–300 km/h, uses traction motor with specifications between 300–1200 kW [16][17][18]. In Indonesia, the Jakarta-Bandung high-speed train is currently being built with a maximum operating speed of 350 km/h which is fully managed by the Chinese government [19]. However, in Indonesia itself there is no research on HST designation IM that accommodates Indonesia HST specification, namely with a speed of 250–300 km/h.

Based on these findings, this research design and optimize a 480 kW SCIM to be applied as a traction

motor of an EMU train. By optimizing the SCIM design, it can achieve maximum efficiency and power factor targets. The 480 kW SCIM is the first EMU-type induction motor for HST in the Indonesian domestic railway manufacturing industry. The design process for a SCIM through stator and rotor slot geometry optimization to get the best motor performance based on efficiency and power factor values with minimum targets that must be achieved. The formulated SCIM design was then validated using the ANSYS Maxwell. The simulation results of the proposed design have been proven to work on target.

This paper is organized as follows. An explanation of the steps in optimizing the design of an induction motor with its mathematical calculations, along with the characteristics of the induction motor as a railway traction motor, is presented in Section II. Section III reviews the results of the design optimization method and is reported along with the electromagnetic-thermal analysis of the optimal solution. Finally, the conclusion and points for some future extensions are given in section IV.

II. Materials and Methods

A. Design stage

IM design is a process of iteration to achieve the expected target. The optimization is completed by analytical or numerical solution techniques. The optimization method uses the initial design and constraints to solve the problem. In science, parametric solutions with limited steps or iterative methods converging to heuristic solutions or algorithms satisfying proximate solutions are used. However, several parameters are allowed to be optimized at the same time. To find the highest performance, this paper uses two optimization steps according to the complete design procedure [20], as shown in Figure 1.

1. Design target setting: The traction motor is used to drive the EMU train. The design must achieve the appropriate performance, such as target torque, maximum power, and shaft speed range.
2. Selection of motor type and size: The selected motor must have high efficiency and be easy to maintain. The size of the motor will affect the speed, torque, and power. A comparison of similar traction motors was conducted, then confirmed with the available space in the bogie of a high-speed EMU train.
3. Mathematical modeling of the technical specifications of the traction motor: The derivation of the equation of the traction motor is used for calculations in obtaining the stator and rotor designs, which are the main components of the traction motor. When selecting the number of poles and slots of the traction motor, it is necessary to consider the rotational speed, harmonic slots in the air gap, and leakage inductance. Then the number of poles selected must be able to be implemented at the targeted speed and torque. In addition, a factor is used in determining the number of

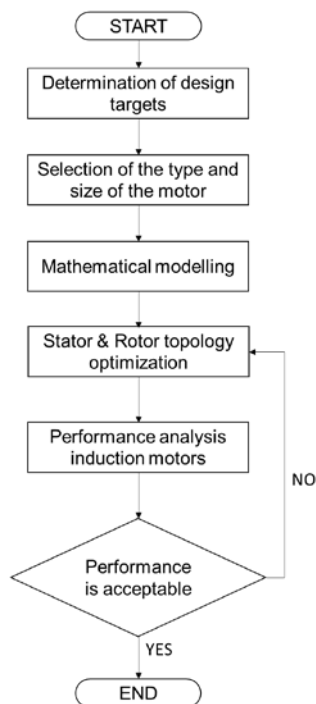


Figure 1. Research methodology flowchart

poles and slots in the traction motor, namely the dimensions motor.

4. Optimization of the stator and the rotor topology: First, the volume size on the stator is calculated. Then, select and count the number of stator slots, the number of slot conductors, coils, and windings. The design of this stator includes the dimensions of the stator slot. Perform the calculation of the length of the air gap. Then, the diameter of the rotor, the number of rotor slots, and the dimensions of the shaft. This rotor design also includes the rotor slot sizes in the selected type.
5. IM performance analysis: IM performance analysis to get an idea of the traction motor design performance. Motor performance assessment is taken from the efficiency and power factor generated when the traction motor is simulated.
6. Design evaluation: Design evaluation is used to determine the feasibility of the traction motor technical specifications that have been prepared.

B. Specification design target

Based on performance requirements and field conditions, the general technical specifications of IM as a traction system can be seen in Table 1. The SCIM design specifications in Table 1 are sourced from similar research and input from expert traction motor engineers. Some of the factors considered in designing an IM are that the motor should have efficiency and power factor according to the requirements for a high starting torque. To achieve the performance, it is necessary to define the details of the induction motor design: the length of the stator, the diameter of the stator, the width of the air gap, the shape of the stator slot, and the rotor slot, and others [21][22]. This process can be seen in the research methodology in Figure 1.

C. Mathematical modelling

The IM calculation uses several stages of the equation [23][24]. Calculation of input from apparent power, as equation (1),

$$S = \frac{h.p.x.0.746}{\eta \cos \phi} = \frac{P}{\eta \cos \phi} \quad (1)$$

where S is apparent power in kVA, P is active power in kW, η is efficiency, and $\cos \phi$ is power factor. Synchronous rotation speed in rpm is calculated with equation (2),

$$n_m = \frac{2.60.f}{p} \quad (2)$$

where n_m is synchronous rotation speed in rpm, f is frequency in Hz, and p is number of poles. Count rated torque, which is defined as equation (3)

$$T_s = \frac{5250 \times S}{n_m} \quad (3)$$

Measuring the main dimensions of the motor, namely the diameter and length of the motor, using equation (4)

$$D^2 l_a = v_T T_s \quad (4)$$

Table 1.
Design specifications of SCIM

Parameter	Type/Value
Type	SCIM
Number of Phases	3 phases
Number of Poles	4 poles
Input voltage	2300 VAC
Output capacity	480 kW
Frequency	85 Hz
Rotational speed	5600 rpm
Cooling	Forced ventilation
Operating temperature	75 °C

where D is stator inner diameter, l_a is stacking length, v_T is volume constant, and T_s is rated torque.

1) Stator topology

Stator bore diameter is defined by equation (5)

$$D = \frac{D_o - 0.647}{1.175 + 1.03/p} \quad (5)$$

where D is stator inner diameter, D_o is outside diameter, and p is number of poles. Determining the number of stator slots through equation (6)

$$S_1 = p \times q \times x \times m \quad (6)$$

where S_1 is the number of stator slots, p is the number of poles, q is the number of pole/slot/phase, and m is the number of phases. Measuring the stator slot pitch, that is the distance measured between the stator gear and the slot along the diameter of the stator hole. Stator slot pitch (λ_1) is obtained through equation (7)

$$\lambda_1 = \frac{\pi D}{S_1} \quad (7)$$

The stator slot width (bs1) obtained by the range of limitations of λ_1 using equation (8)

$$0.5 \lambda_1 \leq bs1 \leq 0.6 \lambda_1 \quad (8)$$

As for getting the stator slot depth (ds1) on the following stator slot width range using equation (9)

$$2bs1 \leq ds1 \leq 4bs1 \quad (9)$$

Based on Figure 2, the width of the stator slot consists of a conductor of coil side and slot liner. The

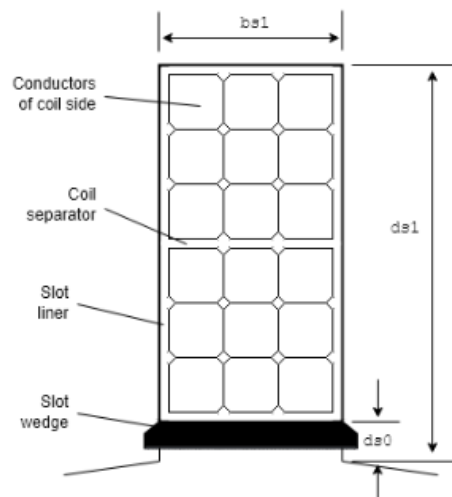


Figure 2. Stator slot design

coil side consists of two sides with a liner slot that functions as ground insulation on the stator slot component. While the height of the slot is composed of a conductor of coil side, coil separator, slot liner, and slot wedge. From Figure 2 to get the stator slot width ($bs1$) and the stator slot depth ($ds1$) in equation (8).

2) Rotor topology

To get the dimensions of the rotor, it begins by determining the number of rotor slots through equation (10)

$$S_1 - S_2 = \pm 3kp \quad (k = 1, 2, 3, \dots) \quad (10)$$

where S_2 is the number of rotor slots. The air gap affects the magnetization of the required current. The distance of the air gap, obtained by equation (11)

$$\delta = 0.2 + 2\sqrt{DL} \quad (11)$$

where δ is air gap distance, D is Stator inner diameter, and L is the stator core length. Rotor diameter (D_r) obtained using equation (12)

$$D_r = D - 2\delta \quad (12)$$

In Figure 3, in designing an IM, it is necessary to pay attention to the rotor width ($br1, br2$) and the rotor depth ($dr1, dr2$). The rotor slot in Figure 3 is designed with the rotor slot open with the width of the rotor bar ($br2$) that must fit to avoid excessive rotor leakage reactance. Designing the rotor slots must be precise so that the cross-sectional area of the rotor rod meets the tolerable current density. The current density of the rotor rod is affected by the height of the rotor bar slot ($dr1, dr2$). Determine the height and width of the rotor slots by using a depth-to-width ratio (rdw) with a range of $3 \leq rdw \leq 6$ through equation (13) and equation (14)

$$br1 = \left(\frac{s_b}{rdw}\right)^{1/2} \quad (13)$$

$$dr1 - dr2 = (rdws_b)^{1/2} \quad (14)$$

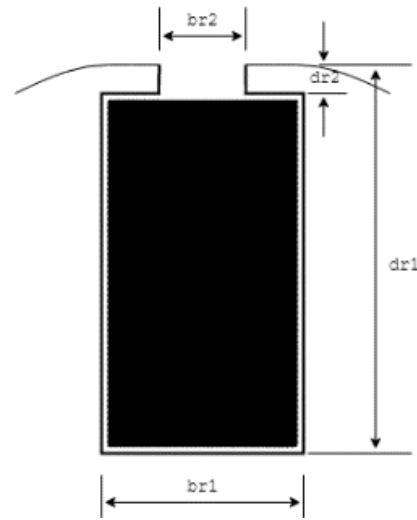


Figure 3. Rotor slot design

where $br1$ is the rotor bar width, $dr1 - dr2$ is the rotor bar depth, rdw is the depth-to-width ratio and s_b is the cross-section area of the rotor bar.

D. Induction motor characteristics

The performance of IM is usually measured on torque and output power. The graph is divided into three parts: when the torque is constant, the power is constant, and the slip is limited, as shown in Figure 4. When the torque region is constant, the voltage-frequency ratio (V/f) is constant; it causes the engine output power to increase linearly proportional to the increase in supply power. When the supply frequency continues to increase, it results in a constant motor current. At the same time, the air gap flux decreases; this condition occurs when the power area is constant. When the slip area is limited, when the engine is operating, it will maximize the torque output and reduce the motor's outgoing power. The acceleration of the traction system ability on the incline and maximum speed is characteristic of the torque and power of the induction motor [24][25].

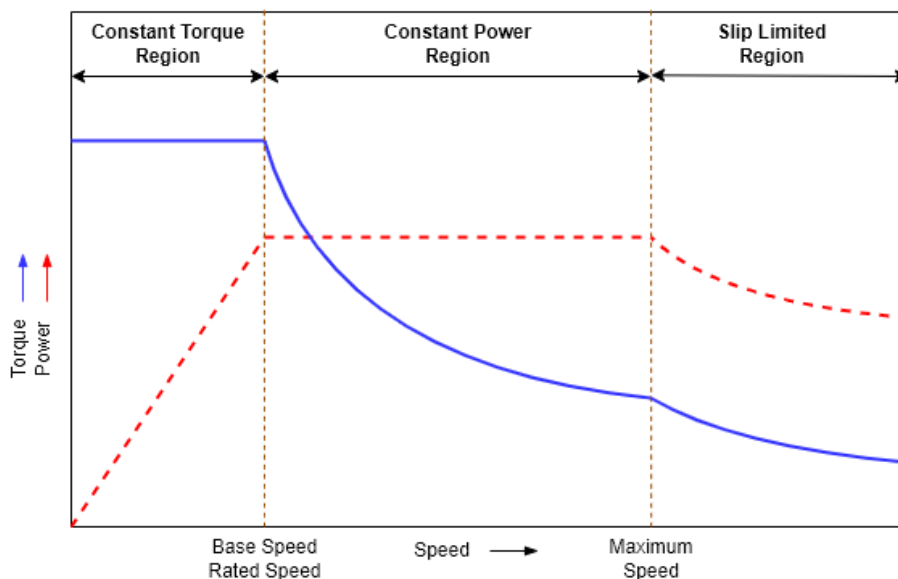


Figure 4. Induction motor performance characteristics

As an electric traction system, the induction motor must meet the following requirements: starting and rising at low speed, it should have high torque, while at high speed in the cruising area, it should have high power; fast torque response with high efficiency when the speed and torque range is wide; reliable and resistant in various operating conditions of the train and when regenerative braking has high efficiency [26][27].

The characteristics of IM performance measured by ANSYS Maxwell are power factor, efficiency, and developed torque. The input power factor is equation (15)

$$PF = \cos(\angle \bar{U}_1 - \angle \bar{V}_1) \quad (15)$$

PF is the power factor, $\angle \bar{U}_1$ is phase voltage angle, and $\angle \bar{V}_1$ is phase current angle. The efficiency is the percentage ratio of output and input power using equation (16)

$$\eta = \frac{P_o}{P_i} \times 100\% \quad (16)$$

η is efficiency, P_o is output power, and P_i is input power. Developed torque is obtained by dividing developed power by shaft speed using equation (17)

$$T_d = \frac{P_d}{\omega_m} \quad (17)$$

T_d is developed torque, P_d is developed power, and ω_m is shaft speed.

Requirements on the design of the 480-kW SCIM:

- $\eta \geq 90\%$
- $PF \geq 0.85$
- $P_{out} = 480 \text{ kW}$

III. Results and Discussions

A. Initial design

The design specifications of the SCIM in Table 1 are then simulated and validated. This motor is given a dimension limitation of 500 mm. The minimum requirement for the motor is an efficiency value of 90% with a minimum power factor of 0.85. Then the motor is modeled using the derivation results of equation (1) until equation (17). So that from the results of the mathematical modeling above, we get the geometric dimensions of the stator slots and rotor slots.

Figure 5 is a description of the cross-sectional geometry type of the stator slots, where in ANSYS RMxpert module is referred to type 6. This model is used because it makes it easier in production or manufacturing. In the stator slot optimization test,

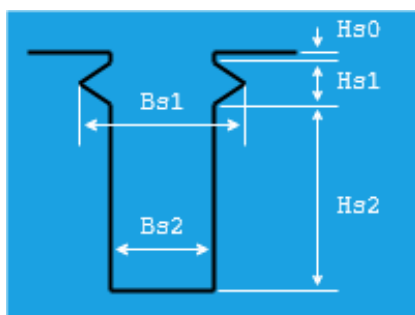


Figure 5. Stator slot geometry type

Table 2.
Stator slot dimension

Name	Value	Unit
Hs0	0.4	mm
Hs1	3.2	mm
Hs2	40	mm
Bs1	16	mm
Bs2	13	mm

Table 3.
Rotor slot dimension

Name	Value	Unit
Hr0	3	mm
Hr1	0	mm
Hr2	43	mm
Br0	4	mm
Br1	7	mm
Br2	7	mm
Air gap	1	mm

the variables that must be considered are Hs0, Hs1, Hs2 as the height of the stator slot. The stator slot widths are Bs1 and Bs2. Table 2 being the stator slot design specification to be verified and validated is obtained from equation (8) and equation (9). The dimensions of the stator slots in Table 2 are obtained from the calculation of the parts of the slot stators, which can be seen in Figure 2.

Furthermore, in the motor design, the cross-sectional geometry type of the rotor slot from type 4 in ANSYS RMxpert is shown in Figure 6. In the rotor slot, the height of the rotor is divided into three parts, namely Hr0, Hr1, and Hr2. As for the width of the rotor, it consists of Br0, Br1, and Br2. In detail, the dimensions of each variable can be seen in Table 3. Detailed dimensions of the rotor slot are obtained from equation (13) and equation (14).

Based on the SCIM design specification data shown in Table 1, the dimensions of the stator slot in Table 2 and the rotor slots in Table 3, simulations were carried out using ANSYS Maxwell. This simulation is used to obtain SCIM performance values at the initial design. The result indicates that to get an output power of 480 kW; the required input power is 519.78 kW. Then, the efficiency value is obtained 92.35%, PF of 0.90, and mechanical shaft torque of 1807.44 Nm.

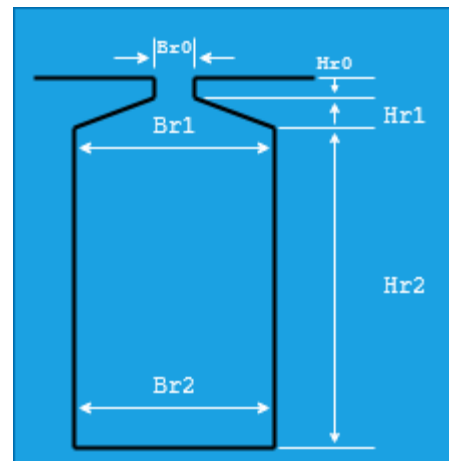


Figure 6. Rotor slot geometry type

Table 4.
Optimize stator slot geometry

No	Hs2	Bs2	Shaft torque (Nm)	η (%)	PF
S1	21	13	1809.50	87.211	0.915
S2	24	13	1808.01	87.143	0.913
S3	33	13	1808.21	91.421	0.904
S4	35	13	1806.76	91.805	0.902
S5	40	13	1807.44	92.353	0.898
S6	44	13	1806.64	92.712	0.895
S7	49	13	1808.79	92.477	0.884

Table 5.
Optimize rotor slot geometry

No	Hr2	Br0	Br1 = Br2	Shaft torque (Nm)	η (%)	PF
R1	35	5	8	1807.87	92.408	0.912
R2	35	5	9	1806.27	92.475	0.915
R3	35	5	10	1803.97	92.527	0.917
R4	39	5	8	1806.29	92.432	0.908
R5	39	5	9	1806.72	92.497	0.912
R6	39	5	10	1805.38	92.547	0.915

B. Optimize stator slot and rotor slot

The iteration to obtain the best IM performance was carried out by changing the design of the stator slot: the size of the depth and width of the stator slot (Hs2 and Bs2), as shown in Figure 5. The Hs2 and Bs2 values are obtained from the range of the stator slot width values (Bs1) function given by equation (8). The value of Bs2 is changed to be the same as Bs1. Design optimization of stator slot width (Bs2) is in the range of $0.5\lambda_1$, $0.55\lambda_1$, $0.6\lambda_1$ according equation (8). Then, the stator slot depth range (ds1) is about the depth of Hs2 obtained from the overall stator slot height size minus the stator wedge slot size. The stator wedge slot is 3.615 mm. Iteration of the motor stator slot design to get the best motor performance in the motor depth range (Hs2), equation (9) with range 2Bs1, 3Bs1, and 4Bs1. The simulations were carried out without changing the rotor slot design shown in Table 3. The simulations results in motor performance characteristics that can be seen in Table 4.

From Table 4, changes in the dimensions of the stator slots (Hs2 and Bs2) affect the efficiency and power factor. With an Hs2 value of 24 mm and a Bs2 of 13 mm, the smallest efficiency value is 87.143 %, but the PF value is 0.913. On the other hand, the largest Hs2 value is 49 mm, with a Bs2 of 13 mm. The highest efficiency value is 92.477 %, with the lowest PF is 0.884.

Then, the Rotor slot design optimization is done to get the best induction motor performance. The variables that affect the rotor design are the width and height of the rotor. The induction motor rotor slot has a bar depth-to-width ratio (rdw) ratio in $3 \leq rdw \leq 6$. An optimization test to get the rotor bar height value is obtained by multiplying the rdw variable per one level, which is 3, 4, 5, and 6. Meanwhile, the rotor width is obtained by dividing rdw by the rotor bar area. The rdw value used has the same variables, namely 3, 4, 5, and 6. The optimization of the rotor slot using the stator slot

design is in Table 2. The simulation results of the design optimized rotor slot can be seen in Table 5.

From Table 5, for the rotor slot design, the optimum design was obtained by setting the motor's efficiency target to above 90 % and PF 0.85. The highest efficiency value is 92.547 %, with a PF value is 0.915. Changes in Hr2, Br0, and Br2 resulted in an efficiency greater than 92 %. Shaft torque is rated at ± 1804 –1806 Nm with a minimum PF in the range of 0.89 to 0.91. The optimized design has reached the minimum required target from this rotor slot simulation.

C. Performance characteristics analysis

Table 6 contains a comparison of motor performance values resulting from the optimization of rotor slots and stator slots. The dimensions of the stator slot and rotor slot in the initial design and S6 resulted in efficiency values of 92.353 % and 92.712 %, with a PF of less than 0.9. Meanwhile, during the optimization of stator slots and rotor slots in S2, the lowest efficiency value was 87.143 %, with a fairly high PF of 0.913. The most optimal geometric dimensions of stator and rotor slots were obtained at R6 with an efficiency value of 92.547 %, PF 0.915, and the lowest rated slip of 0.005. This rated slip value is close to zero, which means that the mechanical rotational speed will approach the synchronous speed in this operation. The simulation uses the ANSYS Maxwell analytical tool to obtain the characteristics of the IM.

Figure 7 shows the visualization of the magnetic flux density and Figure 8 shows flux lines from the most optimal SCIM design (R6). Magnetic flux is defined as the number of magnetic force lines passing through a surface. Figure 7 shows that at a speed of 2539.2 rpm and a rotor position of 83.52 degrees, the largest magnetic flux density value is 2.4286 Tesla. Based on Figure 7 and Figure 8, it can be compared that when the lines of magnetic force increase, the value of the magnetic flux density also increases. The magnetic flux in an induction motor is

Table 6.
Simulation of SCIM

Parameters	Initial design	S2	S6	R6
Stator slot geometry				
Hs0 (mm)	0.4	0.4	0.4	0.4
Hs1 (mm)	3.2	3.2	3.2	3.2
Hs2 (mm)	40	24	44	40
Bs1 (mm)	16	16	16	16
Bs2 (mm)	13	13	13	13
Rotor slot geometry				
Hr0 (mm)	3	3	3	3
Hr1 (mm)	0	0	0	0
Hr2 (mm)	43	43	43	39
Br0 (mm)	4	4	4	4
Bs1 (mm)	7	7	7	7
Bs2 (mm)	7	7	7	7
Performance				
Input power (kW)	519.78	550.68	518.124	518.72
Output power (kW)	480.03	479.88	480.363	480.058
Mechanical shaft torque (Nm)	1807.44	1808.01	1808.64	1805.38
Efficiency (%)	92.353	87.143	92.712	92.547
Power factor	0.899	0.913	0.895	0.915
Rated slip	0.006	0.007	0.006	0.005
Rated shaft speed (rpm)	2536.17	2534.57	2536.22	2539.2

generated from the current flowing in the stator coil. The magnitude of the current that varies at any time on each phase in the stator coil produces a different magnetic flux, as seen in Figure 7. There are areas with different colors. With the magnetic flux in the stator coil, a current will be induced in the rotor, as shown in the magnetic flux line in Figure 8. As a result of the current in the rotor and the magnetic field in the stator, it can rotate the rotor.

Figure 9 shows the value of the magnetic flux density in the air gap between the stator and rotor sections. The magnetic flux density at the ends of the stator and rotor can reach a value of 2.4286 Tesla, which is the largest value. This can be due to the largest magnetic field induction found in that part. In the air gap section, there is also a magnetic flux value because that section is also passed by magnetic field lines.

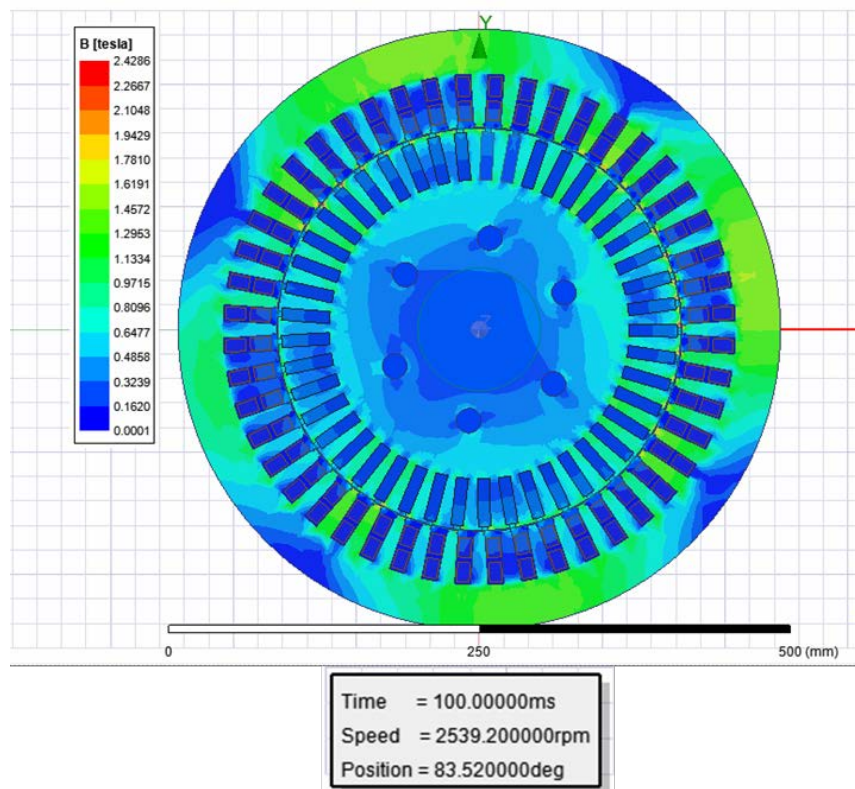


Figure 7. Magnetic flux density of the IM design

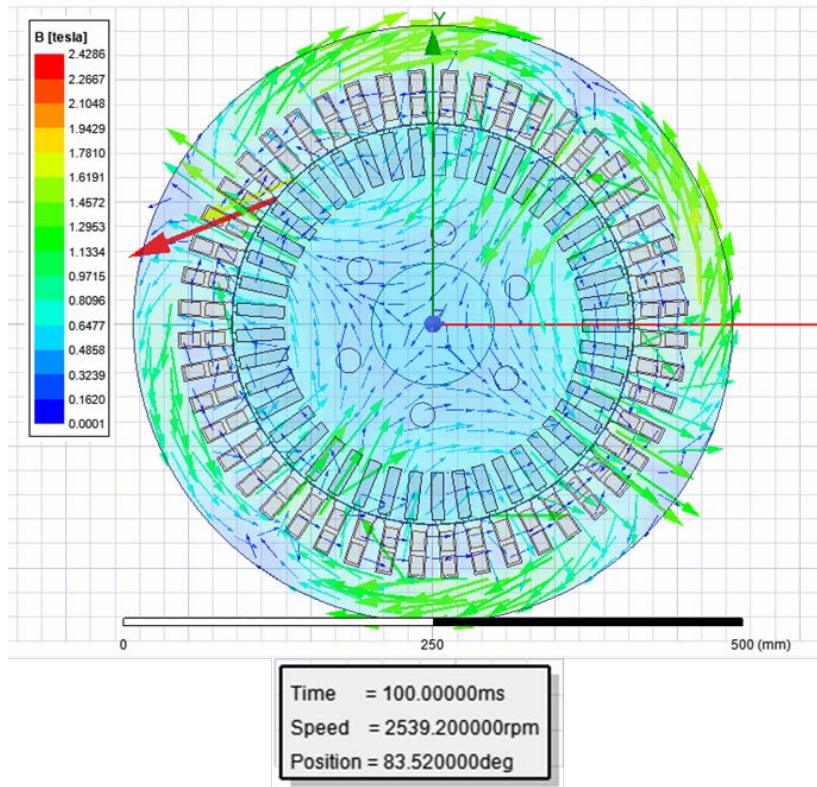


Figure 8. Magnetic flux lines of the IM design

Figure 10 shows the graph of the flux linkage on the stator coil of an SCIM R6 in Table 6. Flux linkage is defined as the value of the magnetic flux through a coil. The graph shows an average linkage flux value of ± 3.20 Wb. In addition, it can be observed that there is a shift in the phase angle due to the difference in the phase angle of the current flowing in the stator coil in the form of a 3-phase electric current.

Figure 11 shows the graph of core loss on an SCIM R6. Core loss is defined as losses in iron which is the total of Eddy current losses, hysteresis losses, and additional/excess losses. Based on the graph in Figure 5, it can be observed that at the beginning of

the rotation, the core loss value is high, and it decreases when it reaches a steady state.

Figure 12 shows the graph of the losses in the SCIM R6 design such as the core loss is losses in iron, the solid loss is electrical losses for “solid” or “single” type conductors, the stranded loss is ohmic or resistance losses of “stranded” type conductors for a 3-phase machine, and mechanical loss in the simulation is losses in the shaft of the motor. In Figure 12, it can be observed that the value of the losses fluctuates at the beginning of the motor rotation and decreases when it reaches a steady state.

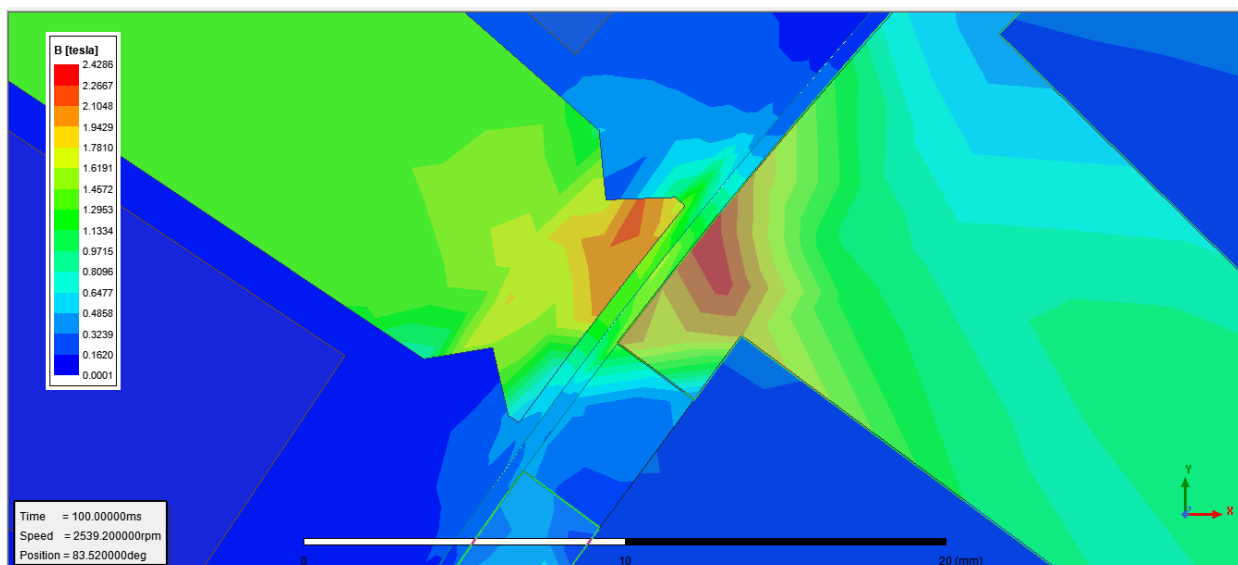


Figure 9. Air gap flux density of the IM design

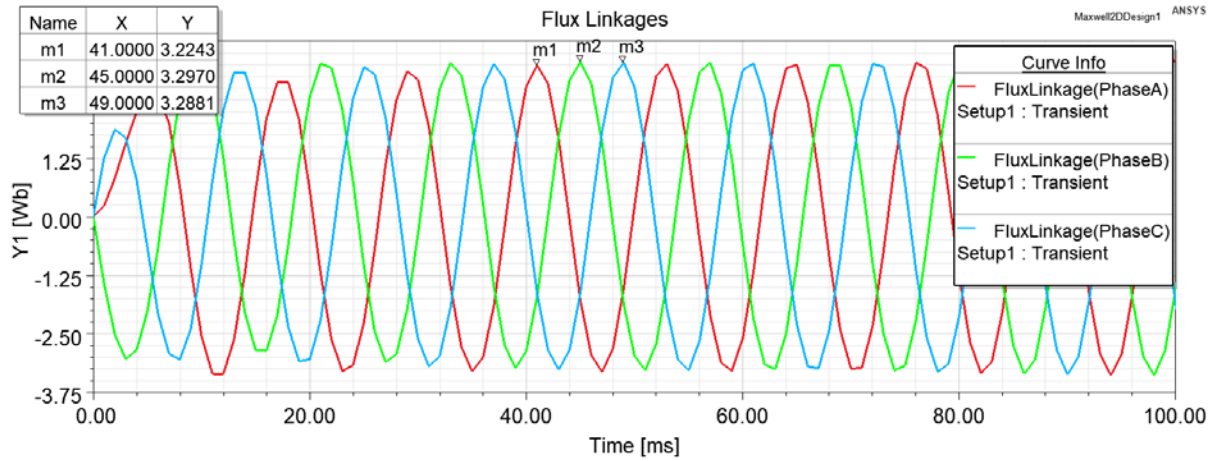


Figure 10. Flux linkages of the IM design

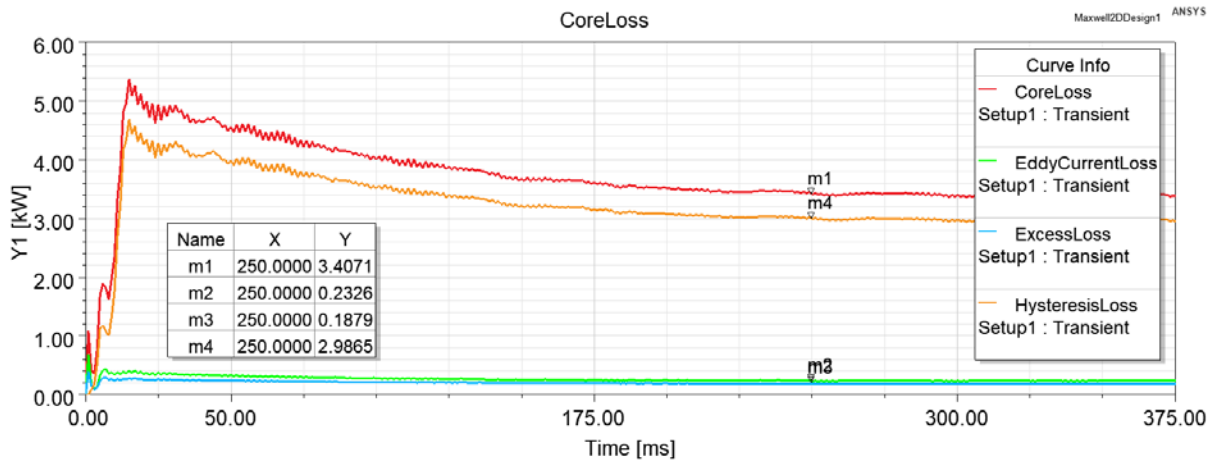


Figure 11. Core loss of the IM design

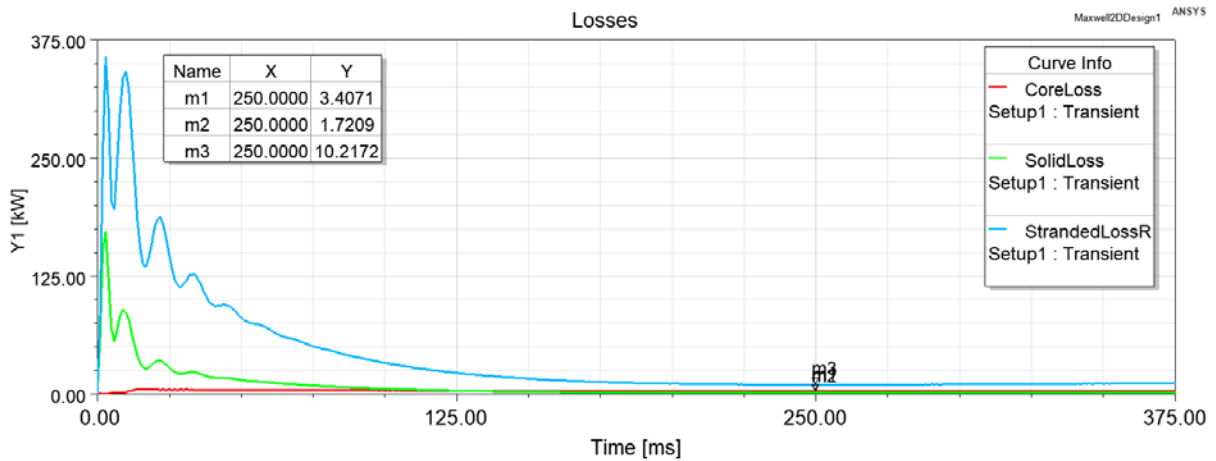


Figure 12. Losses of the IM design

Figure 13 shows the average loss value of the SCIM R6 design. The average total motor losses value is 16.8167 kW. The average total loss value is the sum of the average core loss, solid loss, stranded loss, and mechanical loss, as shown in Table 7. Basically, the calculation of the core loss depends on the particular steel type and the sheet thickness. The solid loss depends on the distribution of the eddy current density and stranded loss depends on the resistances of the coils that influence of coil wire length and wire cross-section. The performance characteristics of the torque-speed motor is shown

in Figure 14. When the speed is low, between 115 to ± 2500 rpm, which indicates a constant torque region, the torque is in a high and constant condition of

Table 7. Motor induction losses

No	Losses	Value (kW)
1	Average core loss	3.3913
2	Average solid loss	2.0772
3	Average mechanical loss	0
4	Average stranded loss	11.3482
	Average total losses	16.8167

±1800 Nm. Then, it decreases when the speed is above 2500 rpm. In Figure 15, the power-speed performance shows three states. When the speed is 115 to ±2500 rpm, the power increases from 21 to 480 kW. When the power increases from 2500 rpm to 4100 rpm, the power states at a constant value

480 kW at constant power region. Then, the rotational speed is above 4929 rpm; the power shows a downward trend representing slip limited region.

Besides that, ANSYS Maxwell produces a flat cross-sectional shape from SCIM which can be seen

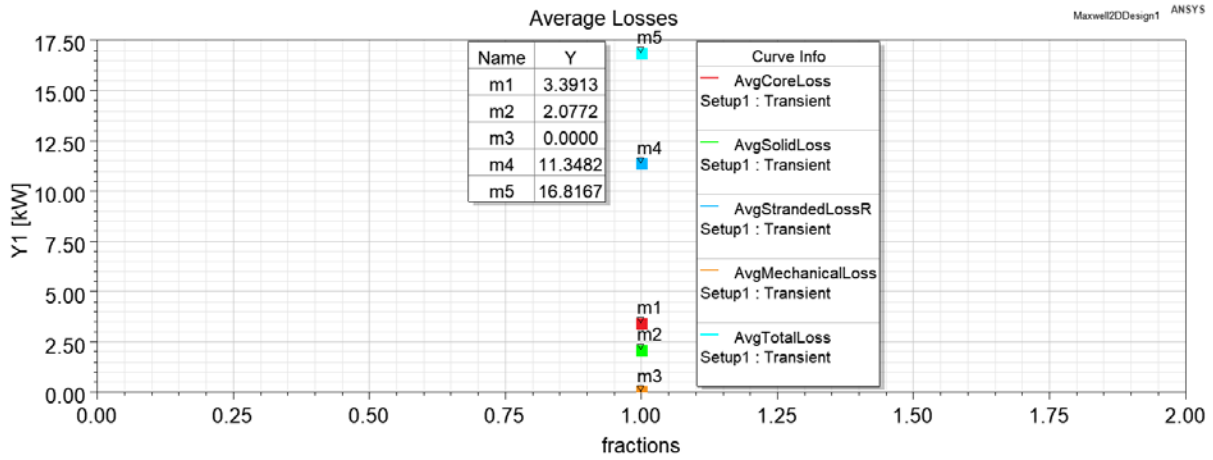


Figure 13. Average losses of the IM design

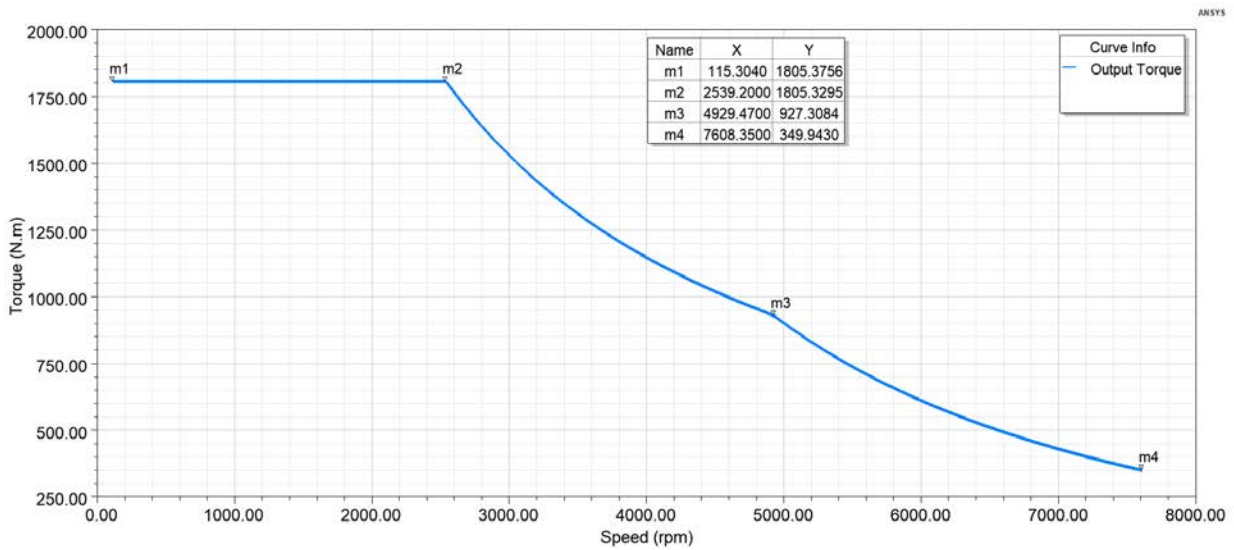


Figure 14. Torque-speed characteristics of the optimal IM design

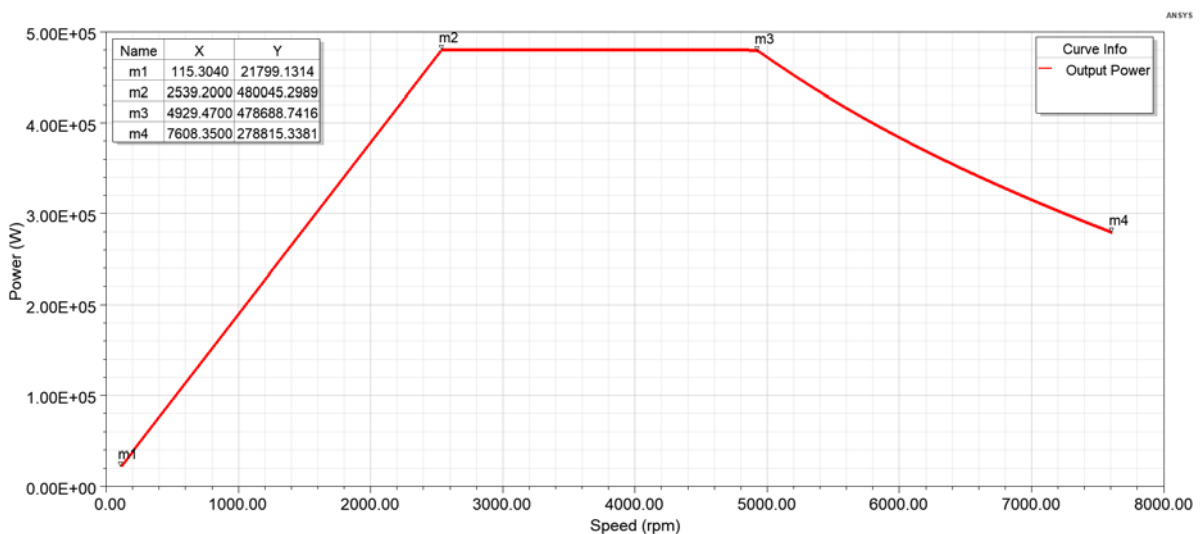


Figure 15. Power-speed characteristics of the optimal IM design

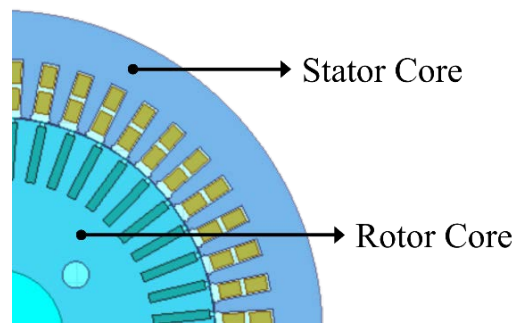


Figure 16. SCIM flat cross section

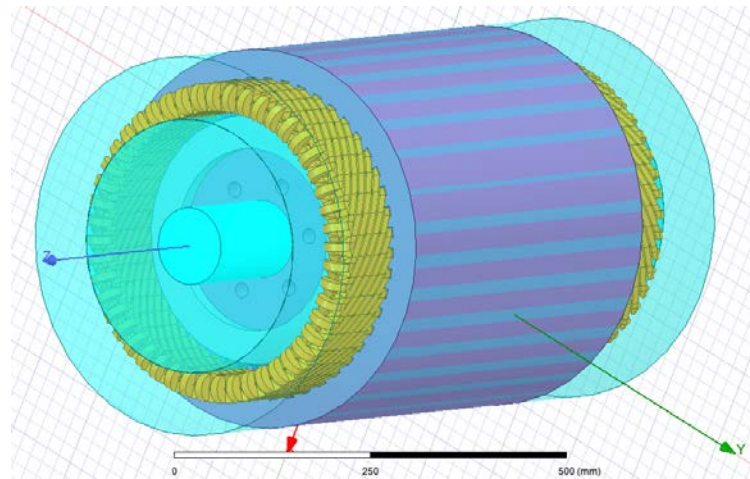


Figure 17. 3D model of SCIM

in Figure 16. The figure shows the core part of SCIM consists of stator cores and rotor cores. A comprehensive 3D model of the SCIM has been created too, which can be seen in Figure 17. The simulation shows a visualization of the dimensions of the stator, rotor, winding stator, rotor bar, and shaft parts.

IV. Conclusion

In this research, we have shown that the In this paper, the SCIM design has been conducted by optimizing the stator slot and rotor slot design to get efficiency and power factor targets. The motor with specifications: 3-phase, 4-pole, 480 kW output power, 2300 VAC input voltage operated at a frequency of 85 Hz. This design has been simulated using ANSYS Maxwell. The stator-rotor slot design is optimized by changing the stator-rotor slot size based on each parameter's range limit. From the simulation, it is found that optimization on the rotor slot affects the efficiency of the motor to be better than optimization on the stator slot. The best SCIM performance value obtained is a size geometry slot stator Hs0 of 0.4 mm, Hs1 of 3.2 mm, Hs2 of 40 mm, Bs1 of 16 mm, and Bs2 of 13 mm. The geometry size of the rotor slot is Hr0 of 3 mm, Hr1 of 0 mm, Hr2 of 39 mm, Br0 of 5 mm, Br1 of 10 mm, and Br2 of 10mm. From the size of the stator slot and the rotor slot dimensions, the obtained efficiency is 92.547 % with a power factor of 0.915, a rated shaft speed of 2536.17 rpm, and a rated slip of 0.005. The data shows the highest efficiency value, the optimal

power factor value, with the smallest slip rated value. From the optimization to get the best SCIM design performance, the minimum losses are obtained and produce the optimal dimension of SCIM. Hopefully, the result from this study can be developed and applied in the Indonesian domestic railway manufacturing industry, especially for EMU trains.

Acknowledgements

This work was partly supported by Research Center for Transportation Technology and Research Center for Process and Manufacturing Industry Technology, National Research and Innovation Agency, Indonesia.

Declaration

Author contribution

H. Luthfiyah: Writing - Original Manuscript, Writing - Review & Editing, Conceptualization, Formal Analysis, Investigation, Visualization, Supervision. O.A. Qowiy: Writing - Original Draft, Writing - Review & Editing, Conceptualization, Investigation, Validation, Data Curation. A.I. Malakani: Formal Analytics, Resources, Software, Conceptualization, Data Curation, Visualization, Reviewing & Editing. D.H. Arthanto: Formal Analysis, Resources, Software, Conceptualization, Visualization. F.D. Setiawan: Formal Analysis, Resources, Software, Visualization, Writing - Review & Editing. T.A. Ramanel: Formal analysis, Resources. G.M. Putra: Formal Analysis, Resources, Software, Review & Editing. S. Kamar: Formal Analysis, Resources, Oversight, Funding Acquisition. A.A. Suryandi: Review & Editing, Supervision.

Funding statement

This research did not receive any specific grant from funding agencies in the public, commercial, or not-for-profit sectors.

Competing interest

The authors declare that they have no known competing financial interests or personal relationships that could have appeared to influence the work reported in this paper.

Additional information

Reprints and permission: information is available at <https://mev.lipi.go.id/>.

Publisher's Note: National Research and Innovation Agency (BRIN) remains neutral with regard to jurisdictional claims in published maps and institutional affiliations.

References

- [1] K. Sato, H. Kato, and T. Fukushima, "Outstanding Technical Features of Traction System in N700S Shinkansen New Generation Standardized High Speed Train," *IEEJ Journal of Industry Applications*, vol. 10, no. 4, pp. 402–410, 2021.
- [2] Z. Wu, C. Gao, and T. Tang, "An Optimal Train Speed Profile Planning Method for Induction Motor Traction System," *Energies (Basel)*, vol. 14, no. 16, p. 5153, Aug. 2021.
- [3] S. Nategh, D. Lindberg, R. Brammer, A. Boglietti, and O. Aglen, "Review and Trends in Traction Motor Design: Electromagnetic and Cooling System Layouts," in *2018 XIII International Conference on Electrical Machines (ICEM)*, pp. 2600–2606, 2018.
- [4] W. Cai, X. Wu, M. Zhou, Y. Liang, and Y. Wang, "Review and Development of Electric Motor Systems and Electric Powertrains for New Energy Vehicles," *Automotive Innovation*, vol. 4, no. 1, pp. 3–22, 2021.
- [5] S. Nategh et al., "A Review on Different Aspects of Traction Motor Design for Railway Applications," *IEEE Trans Ind Appl*, vol. 56, no. 3, pp. 2148–2157, 2020.
- [6] J. Liang, J. W. Jiang, B. Bilgin, and A. Emadi, "Shaft Design for Electric Traction Motors," *IEEE Transactions on Transportation Electrification*, vol. 4, no. 3, pp. 720–731, 2018.
- [7] R. Ikeda, S. Yusya, and K. Kondo, "Study on Design Method for Increasing Power Density of Induction Motors for Electric Railway Vehicle Traction," in *2019 IEEE International Electric Machines & Drives Conference (IEMDC)*, pp. 1545–1550, 2019.
- [8] S. Enache, A. Campeanu, M. A. Enache, I. Vlad, and M. Popescu, "New Aspects in Optimal Design of Asynchronous Motors used in Light Railway Traction," in *2020 International Symposium on Power Electronics, Electrical Drives, Automation and Motion (SPEEDAM)*, pp. 606–611, 2020.
- [9] A. A. Suryandi, C. S. A. Nandar, D. R. Mandasari, and K. Yulianto, "A 250 kW Three Phase Induction Motor Design for Electric Bow Thruster," in *2018 International Conference on Electrical Engineering and Computer Science (ICECOS)*, pp. 247–252, 2018.
- [10] T. M. Masuku, R.-J. Wang, M. C. Botha, and S. Gerber, "Design Strategy of Traction Induction Motors," in *2019 Southern African Universities Power Engineering Conference/Robotics and Mechatronics/Pattern Recognition Association of South Africa (SAUPEC/RobMech/PRASA)*, pp. 316–321, 2019.
- [11] F. D. Wijaya, I. Imawati, M. Yasirroni, and A. I. Cahyadi, "Effect of different core materials in very low voltage induction motors for electric vehicle," *Journal of Mechatronics, Electrical Power, and Vehicular Technology*, vol. 12, no. 2, pp. 95–103, Dec. 2021.
- [12] X. Sun, Z. Shi, and J. Zhu, "Multiobjective Design Optimization of an IPMSM for EVs Based on Fuzzy Method and Sequential Taguchi Method," *IEEE Transactions on Industrial Electronics*, vol. 68, no. 11, pp. 10592–10600, 2021.
- [13] A. Setiyoso, H. Hindersyah, A. Purwadi, and A. Rizqiawan, "Design of traction motor 180kW type SCIM for KRL (EMU) Jabodetabek re-powering project," in *2014 International Conference on Electrical Engineering and Computer Science (ICEECS)*, pp. 341–344, 2014.
- [14] A. Setiyoso, K. Hadi, L. N. Mulyani, R. Sipahutar, and Y. P. P. Kesawa, "Design of Traction Motor 100kW for LRT Rolling Stock in Jabodetabek – Indonesia," in *2022 7th International Conference on Electric Vehicular Technology (ICEVT)*, pp. 153–156, 2022.
- [15] A. S. Hartono, Roosdiatmoko, T. Widodo, A. Iswanto, Y. Haroen, and P. A. Dahono, "Development of new drive system of diesel electric multiple unit (DEMU) for Indonesia railway," in *4th IEEE International Conference on Power Electronics and Drive Systems. IEEE PEDS 2001 - Indonesia. Proceedings (Cat. No.01TH8594)*, vol. 2, pp. 489–493, 2001.
- [16] M. Torrent, J. Perat, and J. Jiménez, "Permanent Magnet Synchronous Motor with Different Rotor Structures for Traction Motor in High Speed Trains," *Energies (Basel)*, vol. 11, no. 6, p. 1549, Jun. 2018.
- [17] H. Zhao, J. Liang, and C. Liu, "High-Speed EMUs: Characteristics of Technological Development and Trends," *Engineering*, vol. 6, no. 3, pp. 234–244, 2020.
- [18] G. Wu et al., "Pantograph–catenary electrical contact system of high-speed railways: recent progress, challenges, and outlooks," *Railway Engineering Science*, vol. 30, no. 4, pp. 437–467, 2022.
- [19] A. Purba, "The Challenge Of Developing High-Speed Rail Projects: Recent Evidence From Developing Countries," *International Journal of GEOMATE*, vol. 18, no. 70, pp. 99–105, 2020.
- [20] D.-K. Lee and J.-S. Ro, "Analysis and Design of a High-Performance Traction Motor for Heavy-Duty Vehicles," *Energies (Basel)*, vol. 13, no. 12, p. 3150, Jun. 2020.
- [21] M. J. Akhtar and R. K. Behera, "Optimal design of stator and rotor slot of induction motor for electric vehicle applications," *IET Electrical Systems in Transportation*, vol. 9, no. 1, pp. 35–43, Mar. 2019.
- [22] P. Irasari, K. Wirtayasa, P. Widiyanto, M. F. Hikmawan, and M. Kasim, "Characteristics analysis of interior and inset type permanent magnet motors for electric vehicle applications," *Journal of Mechatronics, Electrical Power, and Vehicular Technology*, vol. 12, no. 1, pp. 1–9, Jul. 2021.
- [23] J. J. Cathey, *Electric Machines: Analysis and Design Applying Matlab*. McGraw-Hill, 2001.
- [24] I. Boldea and S. A. Nasar, "The Induction Machines Design Handbook," *CRC Press*, 2018.
- [25] N. Zhao and N. Schofield, "An Induction Machine Design With Parameter Optimization for a 120-kW Electric Vehicle," *IEEE Transactions on Transportation Electrification*, vol. 6, no. 2, pp. 592–601, 2020.
- [26] S. J. Rind, M. Jamil, and A. Amjad, "Electric Motors and Speed Sensorless Control for Electric and Hybrid Electric Vehicles: A Review," in *2018 53rd International Universities Power Engineering Conference (UPEC)*, 2018, pp. 1–6.
- [27] K. S. Mohammad and A. S. Jaber, "Comparison of electric motors used in electric vehicle propulsion system," *Indonesian Journal of Electrical Engineering and Computer Science*, vol. 27, no. 1, pp. 11–19, Jul. 2022.